We are IntechOpen,
the world's leading publisher of
Open Access books
Built by scientists, for scientists

4,800
Open access books available

122,000
International authors and editors

135M
Downloads

154
Countries delivered to

Our authors are among the
TOP 1%
most cited scientists

12.2%
Contributors from top 500 universities

WEB OF SCIENCE™

Selection of our books indexed in the Book Citation Index
in Web of Science™ Core Collection (BKCI)

Interested in publishing with us?
Contact book.department@intechopen.com

Numbers displayed above are based on latest data collected.
For more information visit www.intechopen.com

7

Measurement of the Nanoscale Roughness by Atomic Force Microscopy: Basic Principles and Applications

R.R.L. De Oliveira, D.A.C. Albuquerque, T.G.S. Cruz,
F.M. Yamaji and F.L. Leite[1]
Federal University of São Carlos, Campus Sorocaba
Brazil

1. Introduction

Nanoscale science is the study of objects and phenomena at a very small scale and it has been an emerging, interdisciplinary science involving Physics, Biology, Chemistry, Engineering, Material Science, Computer Science and other areas. The main interest in studying in the nanoscale is related to how nanosized particles have different properties than large particles of the same substance. Nanoscale science allow us to learn more about the nature of matter, develop new theories, discover new questions and answers in many areas including health care, energy and technology and also discover how to make new technologies and products that can improve people's life. Although nanoscale science is a recent development in the scientific community, the development of its main concepts happened over a long period of time and the emergence of nanotechnology is related to experimental advances such as the invention of the Scanning Probe Microscope (SPM), a branch of microscopy that captures surface imagery using physical probes that scan the specimen.

SPM was founded with the invention of the Scanning Tunneling Microscope (STM) in 1982 at IBM in Zurich by Binning (Binning et al., 1982). The tip-sample interaction in STM is based on a tunneling electrical current. Although the ability of the STM to image and measure the material surface with atomic resolution has caused a great impact on the technology community, the tip-sample interaction in STM is limited only for good electrical conductor or semiconductor materials. The need of studying other materials led to the development, in 1986, of the Atomic Force Microscopy (AFM) by Binning, Quate, and Gerber (Binnig et al., 1986) that enabled the detection of atomic scale features on a wide range of insulating surfaces.

2. Basic principles

SPM is defined as a specific type of microscopy that uses the basic principle of scanning a surface with a very sharp probe to image and measure properties of material, chemical and

[1] Corresponding Author

biological surfaces. According to the tip-sample interaction the microscopy has a specific name. The two primary forms of SPM are STM and AFM.

The AFM provides a 3D profile on a nanoscale, by measuring forces between a sharp probe (radius less than 10nm) and surface at very short distance (0.2-10nm probe-sample separation). The probe is supported on a flexible cantilever and the AFM tip gently touches the surface and records the small force between the probe and the surface (Wilson & Bullen, 2007). This force can be described using Hooke`s law:

$$F = -k.x \tag{1}$$

Where F = Force; k = Spring constant; x = Cantilever deflection.

The basic components of an AFM are the probe, the cantilever, the scanner, the laser, a data processor and a photodetector as shown in figure 1.

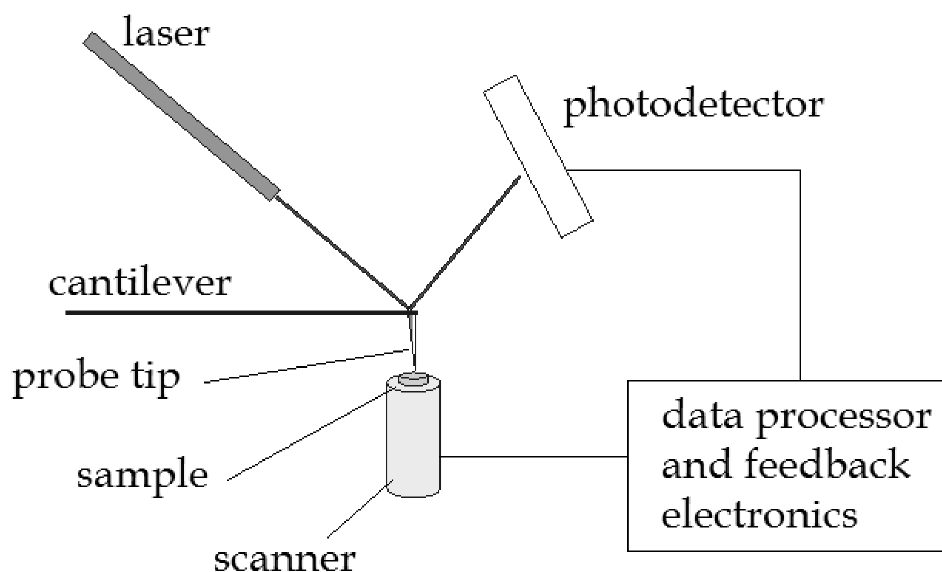

Fig. 1. Principle of AFM.

Forces involved in the tip-sample interaction affect how the probe interacts with the sample. If the probe experiences repulsive forces the probe will be in contact mode otherwise as the probe moves further away from the surface, attractive forces dominate and the probe will be in non-contact mode (Figure 2).

There are three primary imaging modes in AFM: the contact mode where the probe-surface-separation is less than 0.5 nm, the intermittent contact that occurs in a range of 0.5 and 2nm and the non-contact mode where the probe-surface-separation ranges from 0.1 to 10nm.

In contact mode (repulsive regime), if the spring constant of cantilever is less than surface, then the cantilever bends. The force on the tip is repulsive (Figure 3). The forces between the probe and the sample remain constant by maintaining a constant cantilever deflection then an image of the surface is obtained. The advantages of this imaging mode are: fast scanning, good for rough samples and it can be used in friction analysis (Wilson & Bullen, 2007). On the flip side however, forces can damage/deform soft samples (this can be solved by imaging in liquids).

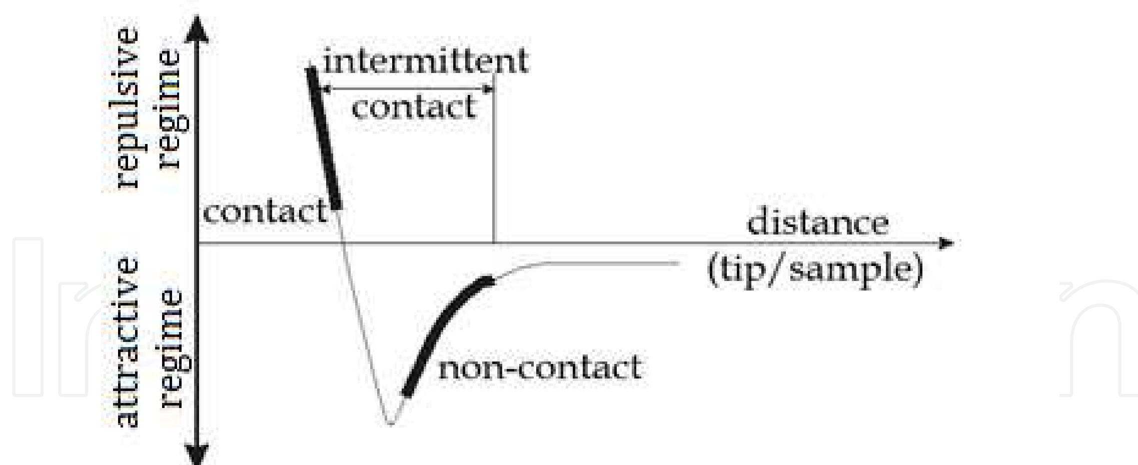

Fig. 2. Force as function of the tip/sample distance. Imaging modes of the AFM based on the type of interaction tip/sample.

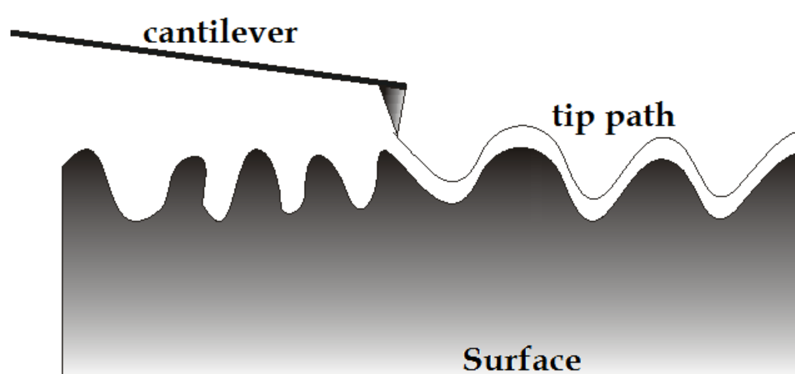

Fig. 3. Contact Mode.

The intermittent mode (Figure 4) is similar to contact but in this mode the cantilever makes intermittent contact with the surface in a resonant frequency (hundreds of KHz). The probe slightly “taps” on the sample surface during scanning, contacting the surface at the bottom of its swing. Because the contact time is a small fraction of its oscillation period, the lateral forces are reduced dramatically. Intermittent mode is usually preferred to image samples with structures that are weakly bound to the surface or samples that are soft (polymers, thin films). There are also two other types of image contrast mechanisms in intermittent mode.

- *Amplitude imaging*: It’s an image contrast mechanism where the feedback loop adjusts the z – piezo so that the amplitude of the cantilever oscillation remains (nearly) constant. The voltages needed to keep the amplitude constant can be compiled into an (error signal) image, and this imaging can often provide high contrast between features on the surface (Wisendanger, 1994)
- *Phase imaging*: The main characteristic of this mode is that the phase difference between the driven oscillations of the cantilever and the measured oscillations can be attributed to different material properties. For example, the relative amount of phase lag between the freely oscillating cantilever and the detected signal can provide qualitative information about the differences in chemical composition, adhesion, and friction properties.

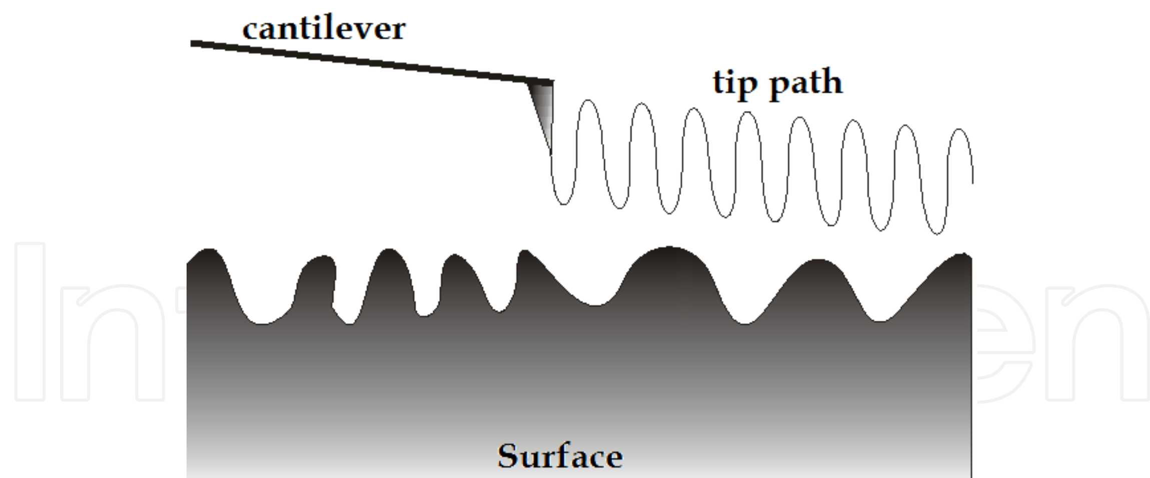

Fig. 4. Intermittent-Contact Mode.

Non-contacting mode (attractive VdW) is based on the knowledge that the probe does not touch the sample but oscillates above it during scanning (Figure 5).

The majority of the samples, unless the ones that are in a controlled UHV (Ultra High Vacuum) or in a environmental chamber have some liquid adsorbed on the surface so the surface topography can be measured by using a feedback loop to monitor changes in the amplitude due to the attractive forces between the probe and the sample.

The advantages of this mode are: very low forces exerted on the samples (10^{-12} N) and extend probe lifetime. The disadvantages of this mode are: generally lower resolution; contaminant layer on surface can interfere with oscillation; usually need UHV to have best imaging.

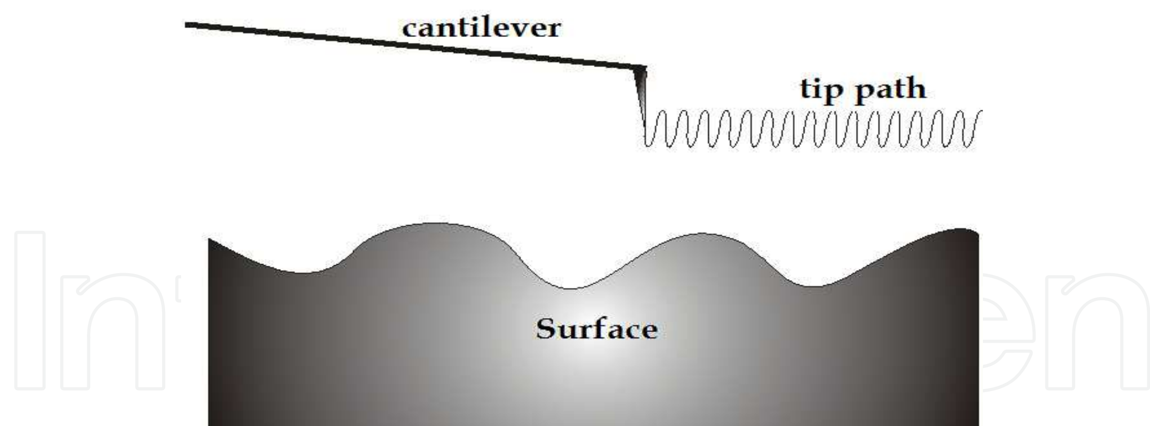

Fig. 5. Non-Contact Mode.

The choice as to which AFM mode to use depends on the surface characteristics of interest and on the hardness/stickiness of the sample. Contact mode is most useful for hard surfaces; a tip in contact with a surface, however, is subject to contamination from removable material on the surface.

Excessive force in contact mode can also damage the surface or blunt the probe tip. Intermittent mode is well-suited for imaging soft biological specimen and for samples with poor surface adhesion (DNA and carbon nanotubes). Non-contact mode is another useful

mode for imaging soft surfaces, but its sensitivity to external vibrations and the inherent water layer on samples in ambient conditions often causes problems in the engagement and retraction of the tip.

3. Surface texture: Roughness, waviness and spacing

Surface texture is an important issue when the main interest is to understand the nature of material surfaces and it plays an important role in the functional performance of many engineering components.

The American National Standards Institute's B46.1 specification defines surface texture as the repetitive or random deviation from the normal surface that forms the three dimensional topography of a surface. Before 1990's the measurement of sample surface was obtained by a contact stylus profiler (Whitehouse et al., 1975) that had limitations including a large stylus radius, a large force and low magnification in the plane and may have misrepresented the real surface topography owing to the finite dimension of the stylus tip (Vorburguer & Raja, 1990). On the ultramicroscopic scale of surface, atomic force microscopy (AFM) has been developed to obtain a three-dimensional image of a material surface on a molecular scale.

"Lay" is the term used to indicate the direction of the dominant pattern of texture on the surface. On a surface, the lay is in the front-to-back direction (Figure 6).

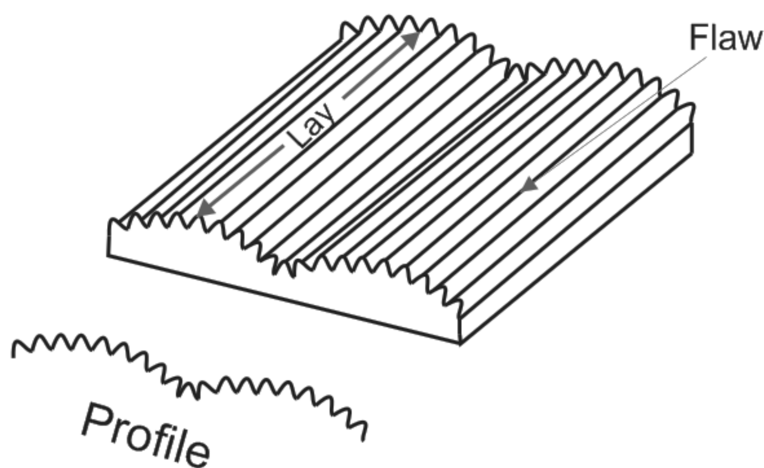

Fig. 6. Surface lay (adapted from B. C. MacDonald & Co., 2011).

Waviness (Figure 7) is the measure of the more widely spaced component of surface texture. It is a broader view of roughness because it is more strictly defined as the irregularities whose spacing, defined as the average spacing between waviness peaks, is greater than the roughness sampling length (Oberg et al., 2000).

There are many parameters for measuring waviness. One of the most important is the waviness evaluation length, which is the length in which the waviness parameters are determined. Within this length the waviness profile is determined. This is a surface texture profile that has the shorter roughness characteristics filtered out, or removed; it also does not include any profile changes due to changes in workpiece geometry. So when it comes to waviness it's important to understand that it's always related to roughness. From this profile the waviness spacing, the average spacing between waviness peaks, is determined.

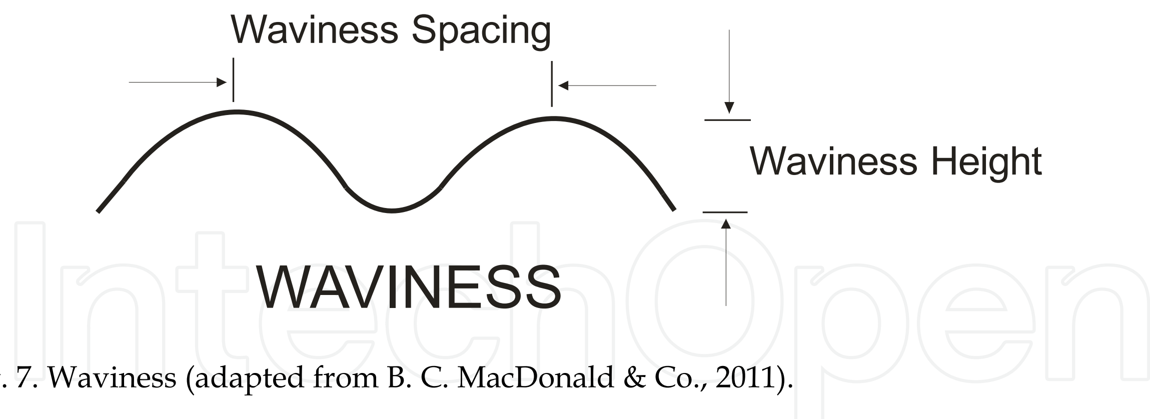

Fig. 7. Waviness (adapted from B. C. MacDonald & Co., 2011).

The waviness height is also determined from the profile, which is just the height from the top of the peak to the bottom of the trough. It is usually at least three times the roughness average height.

Roughness is often described as closely spaced irregularities or with terms such as 'uneven', 'irregular', 'coarse in texture', 'broken by prominences', and other similar ones (Thomas, 1999) (Figure 8). Similar to some surface properties such as hardness, the value of surface roughness depends on the scale of measurement. In addition, the concept of roughness has statistical implications as it takes into consideration factors such as sample size and sampling interval. It is quantified by the vertical spacing of a real surface from its ideal form. If these spacing are large, the surface is rough; if they are small the surface is smooth.

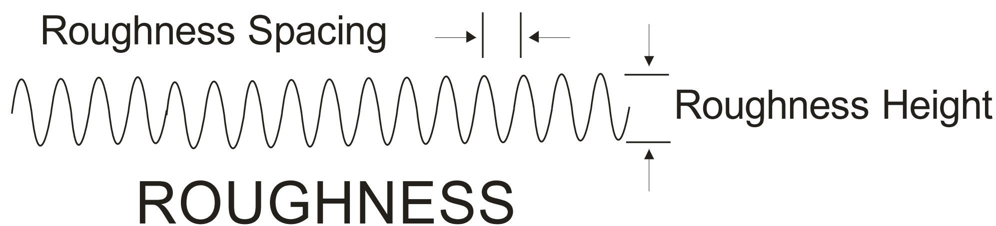

Fig. 8. Roughness (adapted from B. C. MacDonald & Co., 2011).

4. Basic components of AFM

This topic will present some basic ideas about basic components of AFM.

4.1 Scanner

The movement of the tip or sample in the *x*, *y*, and *z*-directions is controlled by a piezo-electric tube scanner, similar to those used in STM. For typical AFM scanners, the maximum ranges are 80 µm x 80 µm in the *x*-*y* plane and 5 µm for the *z*-direction (Figure 9). The scanner moves across the first line of the scan, and back. It then steps in the perpendicular direction to the second scan line, moves across it and back, then to the third line, and so forth. The path differs from a traditional raster pattern in that the alternating lines of data are not taken in opposite directions (Odom, 2004).

While the scanner is moving across a scan line, the image data are sampled digitally at equally spaced intervals. The data are the height of the scanner in z for constant-force mode (AFM) and the data are the cantilever deflection. The spacing between the data points is called the step size. The step size is determined by the full scan size and the number of data points per line. In a typical SPM, scan sizes run from tens of angstroms to over 100 microns and from 64 to 512 data points per line (some systems offer 1024 data points per line.) The number of lines in a data set usually equals the number of points per line. Thus, the ideal data set is comprised of a dense, square grid of measurements.

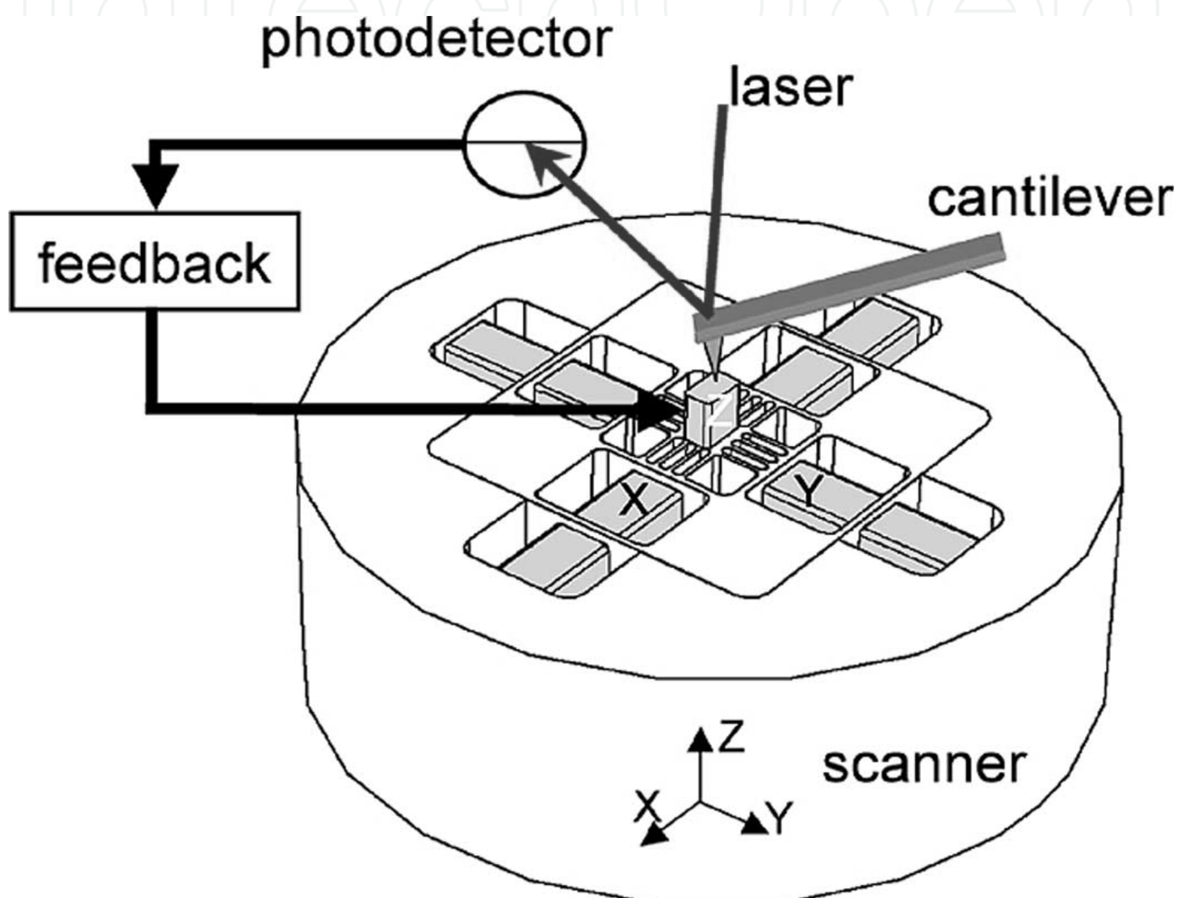

Fig. 9. AFM Scanner (Schitter et al., 2007).

4.2 Probes

The probe is a very important component of a SPM because different probes can measure different properties of the sample (Figure 10). In addition, the probe determines the force applied to the sample. Regarding AFM, the most common probes are the cantilevers that are highly suited to measure the topography of a sample. Different coatings on the cantilevers measure different properties of the sample.

The tip and the cantilever as an integrated component can be fabricated from silicon or silicon Nitride using photolithographic techniques. From a single silicon wafer it is possible to make more than 1000 probes. Regarding the physical properties, the cantilever ranges from 100 to 200 micrometers in length, 10 to 40 micrometers in width, and 0.3 to 2 micrometers in thickness.

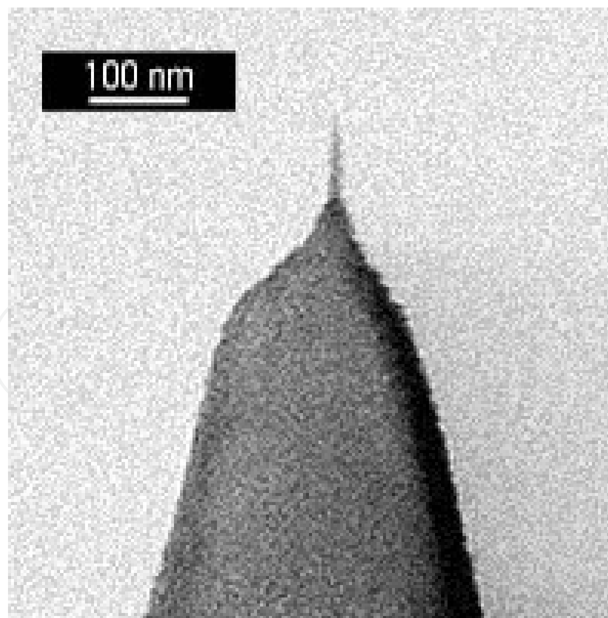

Fig. 10. Probe (1nm radius of curvature HI'RES-W probe – MikroMasch, 2011).

4.3 Properties of cantilever

The spring constant of a cantilever (Figure 11) has a critical importance in atomic force microscopy and it is lower than the spring constant between atoms in a solid, which are on the order of 10 N/m. The spring constant of the cantilever depends on its shape, its dimension and the material from which it's made of. Shorter and thicker cantilevers tend to be stiffer and consequently have higher resonant frequencies. Commercial available cantilevers range over four orders of magnitude, from thousands of a Newton per meter to tens of Newton's per meter. Resonant frequencies range from a few Kilohertz to hundreds of Kilohertz allowing high-speed response for non-contact operation.

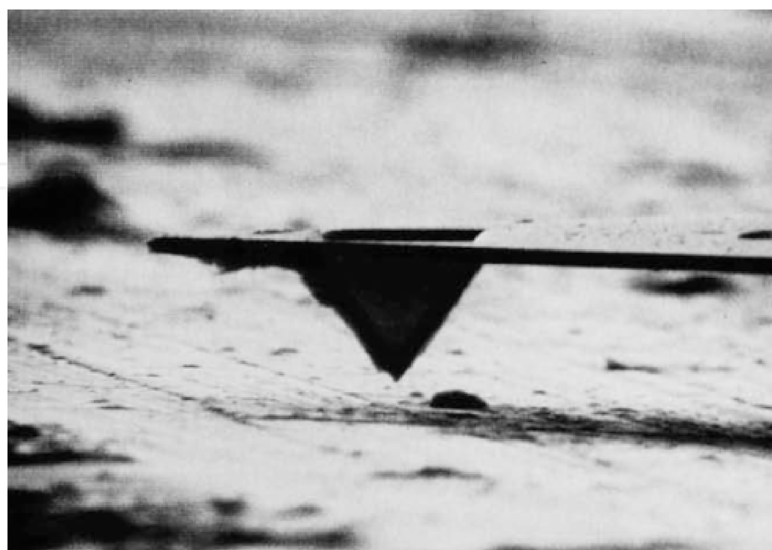

Fig. 11. Microcantilever with microfabricated tip for a contact-mode AFM. This silicon nitride cantilever was manufactured by Park Scientific Instruments, Mountain View, California. (Photograph by Greg Kelderman – Rugar & Hansma, 1990).

4.4 How to select a probe

The desirable properties for a probe are related to the imaging mode and the application. In contact mode, soft cantilevers are preferable because they deflect without deforming the surface of the sample, a silicon nitride microlever would be a good choice for most applications. In non-contact mode, stiff cantilevers with high resonant frequencies give optimal results. For applications other than topography, like MFM (Magnetic Force Microscopy), NSOM (Near-field scanning optical microscopy), SThM (Scanning thermal microscopy) etc., different types of probes have to be used. The probes are available mounted on AutoProbe mounts, mounted on TopoMetrix mounts or unmounted in pre-separated quantities or as a half wafer (Howland & Benatar, 2000).

5. Measurement of surface profile

The characterization of surface topography and its understanding is important in procedures involving friction, greasing and wear (Thomas, 1999). Surface measurement determines surface topography, which is essential for conforming a surface's suitability for a specific function. Surface measurement generally includes surface shape, surface finish and surface roughness. For example, engine parts may be exposed to lubricants to prevent potential wear, and these surfaces require precise engineering— at a microscopic level— to guarantee that the surface roughness holds enough of the lubricants between the parts under compression, so as not to make metal to metal contact. For manufacturing and design purposes, measurement is critical to ensure that the finished material meets the design specification. A profilometer is used to measure surface profile as the surface is moved relative to the contact profilometer's stylus, this notion is changing along with the emergence of numerous non-contact profilometery techniques.

A diamond – sharp stylus is used for the measurement of the surface. The pen is placed on an irregular surface at a constant speed for the variation of surface height with horizontal displacement. According to international standards, a pen may have an angle of 60 and 90 degrees and a tip radius of curvature of 2 microns, 5 or 10. A truncated pyramid is one type with a 90 degree included angle between the opposite sides. It is likely that a profile containing many peaks and valleys with a radius of curvature of 10 microns or less and slopes greater than 45 degrees would be misunderstood by such a stylus (Vorburguer & Raja, 1990).

A very important thing to consider is that the variation of the radius of stylus tip may affect the shape of the profiled surface because the radius of the tip of the pen draws a single envelope of the actual profile. The resolution depends on the real contact between the pen and the actual profile. As the radius stylus is increased contact is made with fewer points on the surface, and therefore the profile is modified. Increasing the radius stylus tends to reduce the measured amplitude of the parameter like Ra (Roughness average). However, the relative effect on roughness is not as great as the peak to valley, and other parameters that are best suited for analysis of sensitive surface structures.

The stylus instruments can be used with two different attachments. The first one has a fixed reference, which limits the movement of the pick-up to a horizontal and the transducer gives the height difference between the instantaneous movement of the pen and the whole pick-up. This is the ideal way to measure the surface profile. Unfortunately, this method requires a setup procedure for leveling by a skilled operator. In order to reduce the setup process, a skid

can be used as second attachment. The skid is one foot blunt that has a large radius of curvature, and it's placed either beyond or behind the stylus. The transducers sense the difference in level between the stylus and the skid. The skid acts as a mechanical filter to attenuate the long spatial wavelength of the surface. As a result of slippage, the wavelength information is long lost. If the long wavelengths are functionally relevant, then the use of a slide should be avoided. In addition, the use of a skid surfaces or surfaces with periodic discrete peaks can result in distortion of the measured profile (Vorburguer & Raja, 1990).

The numerical evaluation of roughness is always preceded by removal of waviness from the measured profile. This is achieved in a surface texture measuring instrument by using an analog or digital filter. In order to exclude waviness, a limiting wavelength has to be specified. This limiting wavelength is referred to as cutoff. The cutoff is given in mm or Inch and the following values are available in many instruments, 0.08, 0.25, 0.8, 2.5, and 8 nm. The cutoff selected must be short enough to exclude irrelevant long wavelength and at the same time long enough to ensure that enough texture has been included in the assessment to give meaningful results. Usually five cutoff settings are used for assessment, and overall traverse length is seven cutoffs (Vorburguer & Raja, 1990).

6. Traditional surface texture parameters and functions (parameters R and S)

The roughness can be characterized by several parameters and functions (such as height parameters, wavelength parameters, spacing and hybrid parameters (Gadelmawla et al., 2002). The following parameters and functions related to the height and spacing (also called parameters R and S) will be discussed as well as their calculation.

6.1 Height parameters (R)

The most significant parameters in the case of roughness are the Height Parameters.

6.1.1 Roughness average

Among Height Parameters, the roughness average (R_a) is the most widely used because it is a simple parameter to obtain when compared to others. The roughness average is described as follows (Park, 2011).

$$R_a = \frac{1}{L}\int_0^L |Z(x)|\,dx \tag{2}$$

Where Z(x) is the function that describes the surface profile analyzed in terms of height (Z) and position (x) of the sample over the evaluation length "L" (Figure 12).

Thus, the R_a is the arithmetic mean of the absolute values of the height of the surface profile Z(x). Many times the roughness average is called the Arithmetic Average (AA), Center Line Average (CLA) or Arithmetical Mean Deviation of the Profile. The average roughness has advantages and disadvantages. The advantages include: ease of obtaining the same average roughness of less sophisticated instruments, for example, a profilometer can provide (R_a); possibility of repetition of the parameter, since it appears very stable statistically, recommended as a parameter for the characterization of random surfaces, it is usually used to describe machined surfaces (B.C. MacDonald & Co, 2011).

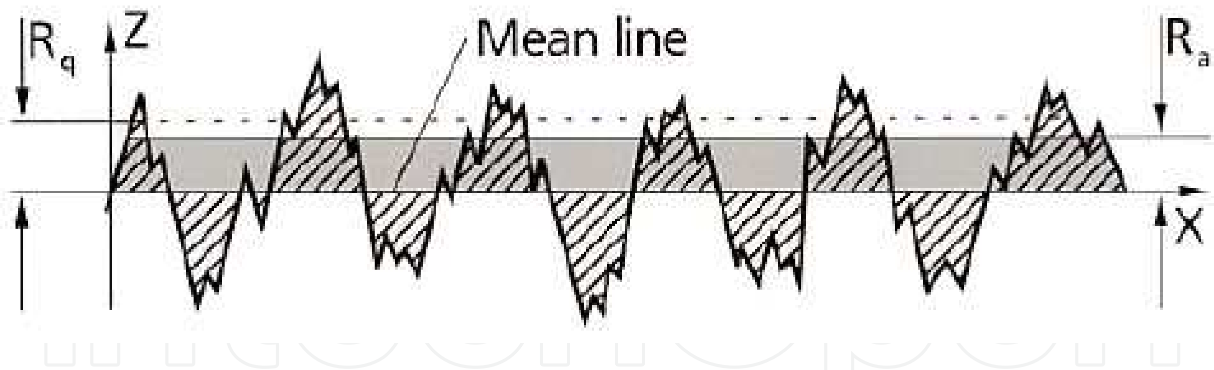

Fig. 12. Profile of a surface (Z). It represents the average roughness R_a and R_q is the RMS roughness based on the mean line (B.C. MacDonald & Co, 2011).

The average roughness, as already said, is just the mean absolute profile, making no distinction between peaks and valleys. Thus it becomes a disadvantage to characterize an average surface roughness if these data are relevant.

The average roughness can be the same for surfaces with roughness profile totally different because it depends only on the average profile of heights. Surfaces that have different undulations are not distinguished (Figure 13). We may have an even surface and some other with peaks (or valleys) with small contributions presenting the same value of average roughness. For this reason, more sophisticated parameters can be used to fully characterize a surface when more significant information is necessary, for example, distinguish between peaks and valleys.

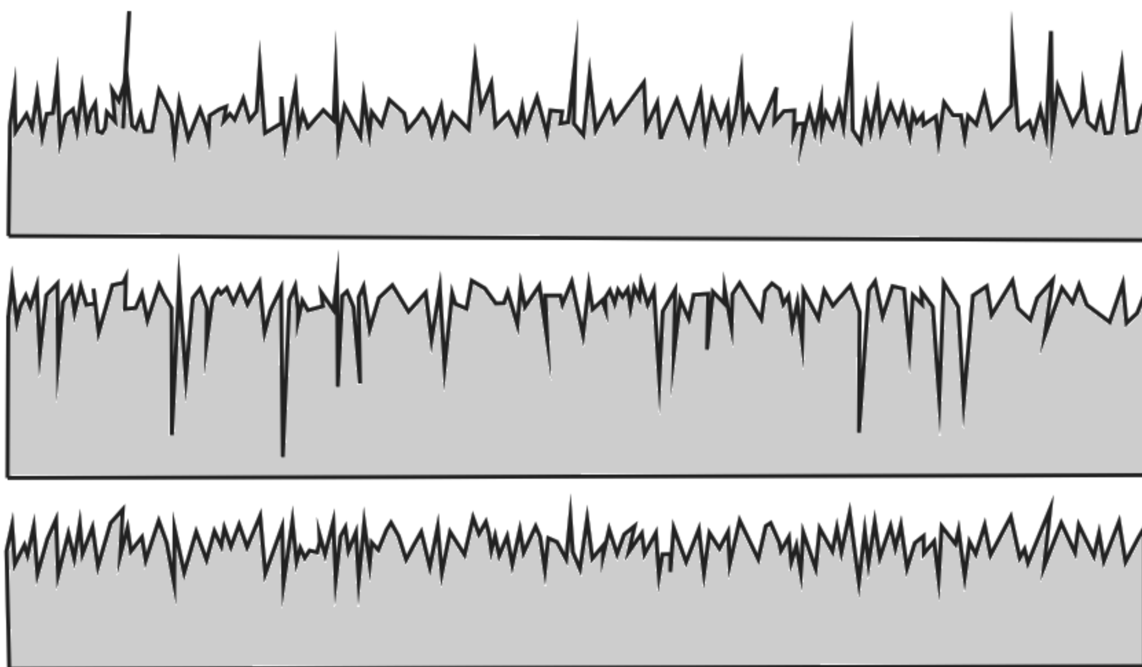

Fig. 13. Different profiles of surfaces, with the same roughness average (adapted from Predev, 2011).

6.1.2 Root mean square roughness (R_q)

The root mean square (RMS) is a statistical measure used in different fields. We cite, as an example, the use of the RMS amplitude applied to harmonic oscillators, such as on an alternating electric current. The root mean square of roughness (R_q) is a function that takes the square of the measures. The RMS roughness of a surface is similar to the roughness average, with the only difference being the mean squared absolute values of surface roughness profile. The function R_q is defined as (Gadelmawla et al., 2002):

$$R_q = \sqrt{\frac{1}{L}\int_0^L |Z^2(x)|\,dx} \tag{3}$$

The software does not need to be sophisticated in order to obtain R_q. For this reason much of the surface analysis equipment (profilometer and SPMs) provides R_q. In SPM, the R_q depends on the swept area of the sample, the scan size.

The R_q is more sensitive to peaks and valleys than the average roughness due to the squaring of the amplitude in its calculation.

6.1.3 Maximum height of the profile (R_T), maximum profile valley depth (R_v) and maximum profile peak height (R_p)

The Maximum Profile Peak Height (R_p) is the measure of the highest peak around the surface profile from the baseline. Likewise the Maximum Profile Valley Depth (R_v) is the measure of the deepest valley across the surface profile analyzed from the baseline (Park, 2011). We can write:

$$R_p = |\max Z(x)| \quad \text{for} \quad 0 \le x \le L \tag{4}$$

$$R_v = |\min Z(x)| \quad \text{for} \quad 0 \le x \le L \tag{5}$$

Thus the Maximum Height of the Profile (R_T) can be defined as the vertical distance between the deepest valley and highest peak.

$$R_T = R_p + R_v \tag{6}$$

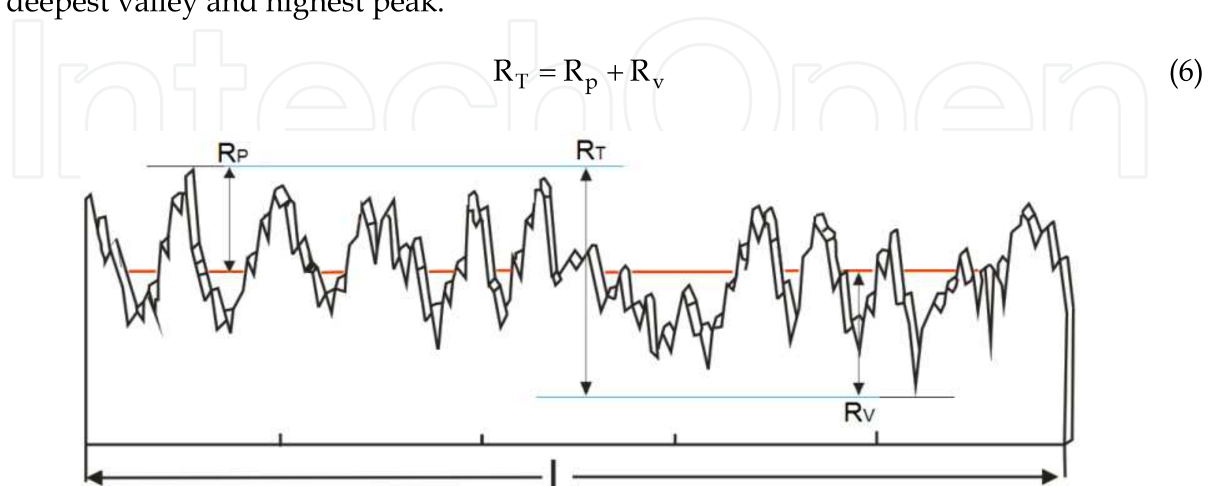

Fig. 14. Illustration of Maximum Height of the Profile (R_T), Maximum Profile Valley Depth (R_v) and Maximum Profile Peak Height (R_p) for the surface profile (adapted from Predev, 2011).

These parameters are useful when trying to find some very sharp peak, which could affect any application of the sample, a scratch or an unusual crack on the material. Often we use the average of these parameters, R_{Tm}, R_{pm} and R_{vm} and comprising the averages along the profile (x) on an evaluation length (L), given by (Park, 2011):

$$R_{pm} = \frac{1}{L}\sum_{i=x}^{L} R_{pi} \tag{7}$$

$$R_{vm} = \frac{1}{L}\sum_{i=x}^{L} R_{vi} \tag{8}$$

$$R_{Tm} = \frac{1}{L}\sum_{i=x}^{L} R_{Ti} = R_{pm} + R_{vm} \tag{9}$$

These average parameters have the same advantage that the extreme parameters described in (4), (5) and (6), but lose accuracy when searching for singularities.

6.1.4 Ten point average roughness - R_z (ISO)

The R_z (ISO) is the arithmetic mean of the five highest peaks added to the five deepest valleys over the evaluation length measured. It is a parameter similar to R_{Tm}.

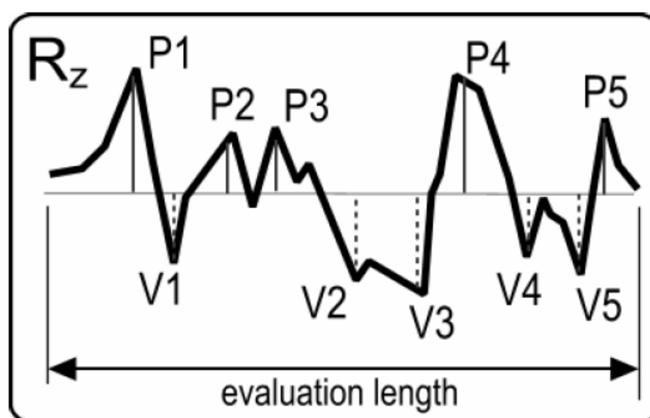

Fig. 15. R_z average of the sum of the five highest peaks in the five deepest valleys of sample's profile (Zygo Corporation, 2011).

6.1.5 Third highest peak to third lowest valley height (R_{3Zi})

The Third Highest Peak to Third Lowest Valley Height is a parameter that overlooks the two highest peaks and the two deepest valleys, taking as measure the vertical variation of the third highest peak from the third deepest valley. The advantage of using this parameter is that it disregards any discrepancies that do not interfere in a meaningful way in the characterization of the surface profile. This ignores the extreme values thus reducing the instability of peaks and valleys. It is a commonly used parameter for the characterization of porous surfaces and sealing surfaces (B.C. Macdonald & Co, 2011).

6.2 Roughness spacing parameters

The Roughness Spacing Parameters are the parameters that relate the roughness to the profile of curling and repetition over a surface.

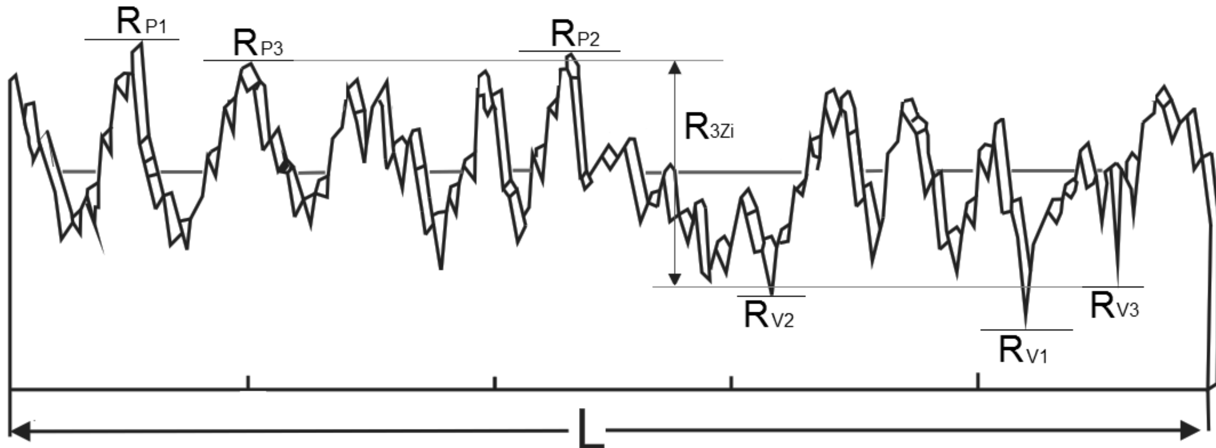

Fig. 16. The two highest peaks (R_{P1} and R_{P2}) and the two deepest valleys (R_{V1} and R_{V2}) are disregarded. The R_{3z}i is counted from the third highest peak (R_{P3}) and the third deepest valley (R_{V3}) (adapted from Predev, 2011).

6.2.1 Peak count

The Peak Count (P_c) is a parameter that provides the count of peaks analyzed along the length L of a surface profile. In this case, the computed peak is the "peak" crossing above an upper threshold and then below the lower threshold. Therefore only values of extreme peaks are significant and establishes a bandwidth in which only peaks and valleys beyond this range will be computed (Park, 2011). The Peak Count is expressed in peaks/inch or peaks/cm (Zygo Corporation, 2011).

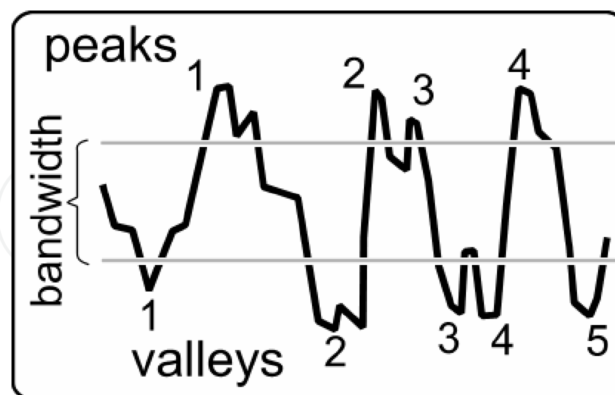

Fig. 17. To determine the peak count only the peaks and valleys that exceed the bandwidth and return are considered (Zygo Corporation, 2011).

6.2.2 Peak density

Peak Density (P_D) represents the density of peaks, i.e., the number of peaks per unit area (Zygo Corporation, 2011).

6.2.3 High spot count

The High Spot Count (HSC) is a parameter similar to the peak count. The main difference between these two parameters is in the defined peak. To be considered a peak in determining the Peak Count, the peak must be followed by a valley that crosses the entire band width (upper and lower threshold). For the High Spot Count, a threshold is set above the average roughness and only the peaks that exceed this one threshold are considered.

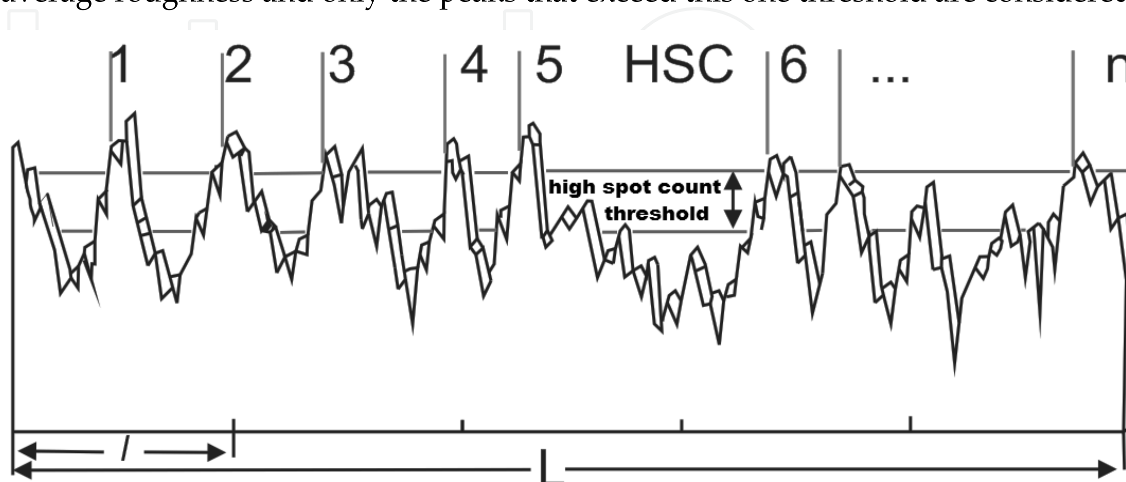

Fig. 18. Illustration of the High Spot Counting and the threshold determining a peak. (Adapted from Park, 2011)

The use of parameters such as Peak Count, Peak Density and High Spot Count has its main application in sheet metal production where the quality control of coatings and paint surfaces is of fundamental importance (B.C. Macdonald & Co, 2011).

6.2.4 Mean spacing

The Mean Spacing (S_m) is the average spacing between peaks in the length of evaluation. In this case the peak is defined as the highest point, along the profile, between a line crossing over the midline and returning below the midline. The spacing between peaks is the horizontal distance between the points where two peaks cross above the midline (Gadelmawla et al., 2002). Thus the mean spacing (S_m) is defined as the average of spacing individual (S_i):

$$S_m = \frac{1}{L}\sum_{i=1}^{L} S_i \qquad (10)$$

The mean spacing (S_m) is generally described in μm or mm.

6.2.5 Average wavelength

The Average Wavelength (λ_a) is a parameter that relates the spacing between local peaks and valleys weighted by their individual frequencies and amplitudes. Thus, the Average Wavelength is given by:

$$\lambda_a = \frac{R_a}{\Delta_a} \qquad (11)$$

Where R_a is the roughness average and Δ_a the mean slope of profile (Park, 2011).

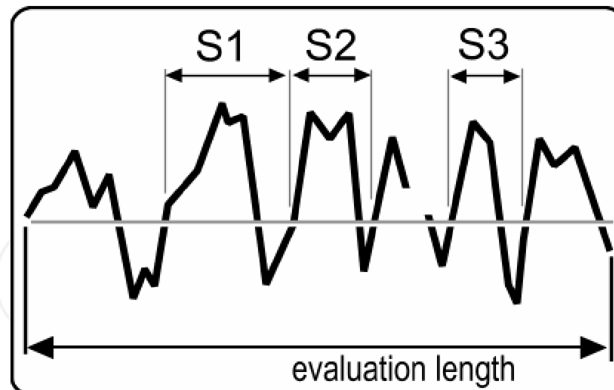

Fig. 19. Three individual spaces in a surface profile. The mean spacing is the average of the three individual spaces on the evaluation length (Zygo Corporation, 2011).

6.2.6 RMS average wavelength

Similar to the R_q and R_a, RMS Average Wavelength (λ_q) takes as reference the root mean square of the spacing between peaks and valleys weighted by their individual frequencies and amplitudes (Park, 2011). RMS Average Wavelength can be calculated by:

$$\lambda_q = 2\pi \frac{R_q}{\Delta_q} \quad (12)$$

Where R_q is the RMS roughness and Δ_q the RMS slope of profile (Park, 2011).

7. Applications (materials)

The roughness is a very significant parameter for various applications. The characterization of materials through its roughness allows one to obtain information on the efficiency of materials in various application areas.

7.1 Electrochemical intercalation

Some materials, usually transition metals oxides, are classified as intercalation materials. These materials are able to receive short radius ions (H+, Li+...) in its network structure via electrochemical techniques (such as cyclic voltammetry and electrochemical impedance spectroscopy). This process is known as electrochemical intercalation.

The electrochemical intercalation is a reversible process, making these materials very interesting in applications where the control over the ability of insertion/extraction of an ion in a structure is essential.

Intercalation materials are commonly used in micro-batteries, smart windows, smart mirrors, displays, gas sensors and other applications. These materials have potential applications due to the possibility of control of their electronic and optical properties.

The electro-physical-chemical properties of intercalation materials are strongly dependent on surface roughness.

The surface roughness acts as a gateway to allocate the ions in the network structure of the material. In collating materials, height and spacing parameters related to roughness are essential to achieve the efficiency of the material (Cruz et al., 2002).

7.2 Dental enamel

The bleaching process can cause variation in the surface roughness of human tooth enamel. These changes are responsible for color changes, glare reduction, opacity.

The surface roughness is responsible for diffuse scattering of light incident on tooth enamel. Thus the surface roughness is an important variable in the bleaching process and must necessarily be considered.

The search for materials that do not significantly increase the roughness of the tooth surface is a challenge in dentistry. Bleaching agents based on nanoparticles of hidroxiapatatia have been shown to be effective by reducing the surface roughness and increasing the brightness of the tooth enamel (Takikawa et al., 2006).

The brightness and surface roughness are closely associated by an inverse correlation. As shown in the figure 20, the gloss increases with decreasing roughness of tooth enamel (Heintze et al., 2006).

7.3 X-ray anode

The anode is the positive electrode in an X-ray tube. It receives the impact of electrons accelerated by the potential difference due to the high voltage applied. The anode is generally made of materials that have high thermal dissipation, such as copper, molybdenum or rhenium. Depending on the x-ray application (i.e. energy of x-ray) a metal coating such as tungsten (W) or molybdenum (Mo) is placed over these thermally dissipative metals at the impact area of the accelerated electrons.

A change in the spectral distribution of X-rays in a cathode ray tube with increasing roughness of the anode has been observed. The increased surface roughness implies an increase of characteristic peaks and a decrease corresponds to the lower energies of the bremsstrahlung spectrum, and an increase in the average energy of beams of X-rays (Nagel, 1988; Stears et al., 1986). The increased surface roughness implies an increase of characteristic peaks and a decreasing in the part corresponding to the lower energies of the bremsstrahlung spectrum. Unlike the filtration process for tungsten (W) where a dip occurs at lower energies (Yoriyaz et al., 2009).

7.4 Polymeric membranes

In the area of environmental protection, a very significant technology is the process of separation by polymeric membranes. Polymeric membranes, such as Polysulfone / Blend Membrane PLURONIC F127, are used to separate the undesired solute in solution. Thus, the active area of the polymer membrane to carry out the process is the surface. The properties related to the surface are important for performing the separation process. Properties such as the pores size distribution, long-range electrostatic interactions and surface roughness are factors that determine the efficiency of polymer membrane for this application.

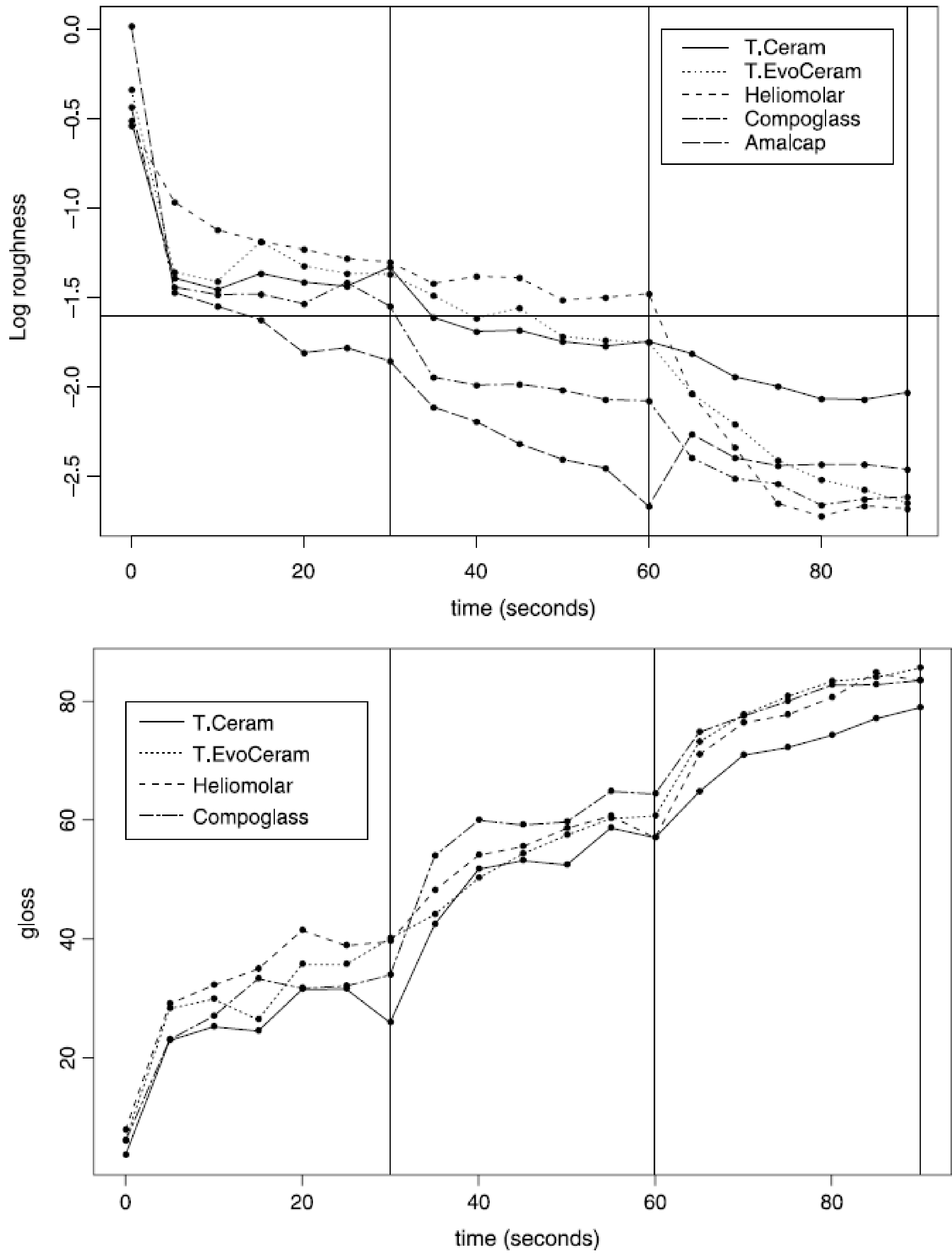

Fig. 20. Relationship between surface roughness and brightness of the teeth treated with five different materials (Heintze & Russon, 2006).

The surface roughness of the polymer membrane is a factor proportional to the bond strength of the membrane. The higher roughness leads to greater adhesive strength of the membrane and greater efficiency in the separation process (Bowen et al., 1998).

8. Effect of RMS roughness on adhesion

In the study of surfaces, related applications to adherence are extremely important. The surface morphology plays a significant effect on adherence. In this section we will discuss the effects that surface roughness plays on adherence.

Adherence is a chemical-physical phenomenon responsible for the union of two surfaces when they come into contact. This union has force of high magnitude in conditions where there is a chemical bond with sharing of electrons, or Coulomb attraction. In some cases the bond strength has relatively low magnitude to occurring by attractive forces of VdW type. The origin of the adhesion force is the same fundamental force of nature responsible for the binding of atoms and molecules.

This phenomenon of interest is multidisciplinary, for example, the effect of adherence on civil engineering projects, cell adhesion in different microorganisms, adhesion of bacteria on the surface of dental enamel, adhesion of polymeric membranes in separation processes for solutes, adhesion of nanoparticles, among others (Bowen et al., 1998).

When contact occurs between two solid bodies, adhesion is not observed. This is due to the fact that much of the surface has a roughness at the microscale. This roughness decreases the area of active interaction between two solid bodies, as only regions with peaks come into contact, thus reducing adhesion.

Liu, D. -L. et al (2007) conducted a study concerning the effect of RMS roughness on the adhesion using AFM. This study provided a better understanding of the effect of roughness on the adhesion when working in the nanoscale. On this scale the effects of adhesion are significant in applications of microelectromechanical systems.

The total adhesion force in this case, the contribution of all molecules involved in the process can be described by the equation (Bowen et al., 1998).

$$F = 2\pi\omega R\left[\frac{R_q}{R+R_q}+\left(\frac{h_c}{h_c+R_q}\right)^2\right] \tag{13}$$

Where: R = tip radius; R_q= RMS of roughness; h_c = distance separating the tip/sample, and $2\pi\omega R$ represents the strength of the AFM system. The total force is normalized by the surface energy so that ω is the work of adhesion force.

The adhesion force falls with increasing surface roughness and also with increasing radius of the tip used in AFM.

9. Complementary analysis: Fractal dimension and power spectral density

Two powerful techniques for further analysis in the study of surfaces are the fractal dimension and Power Spectral Density. These analysis are based on surface roughness. This

type of analysis requires more sophisticated equipment. Most SPMs have image analysis options in their software for additional analysis such as fractal dimension and power spectral density. In this section the analysis will be discussed.

9.1 Fractal dimension

The fractal dimension is a sophisticated parameter used to define the morphology of a surface, considering the roughness present. The surface morphology can be characterized qualitatively by its roughness and its fractal dimension (Guisbiers et al., 2007; Raoufi, 2010; Torkhova & Novikov, 2009; Yadav et al., 2011). The idea of using the concepts of fractal geometry in the study of geometric figures and irregular forms was popularized by Benoit B. Mandelbrot (Mandelbrot, 1982). Since then, such concepts have been used in various fields such as physics, chemistry, biology, materials science, among others.

A fractal is defined by the property of self-similarity or self-affinity, that is, they have the same characteristics for different variations in scale. The thumbnail is like the fractal as a whole and can be classified into self-similar (in the case parts of the fractal is identical to the original fractal) or self-affine (when parts of the fractal is statistically similar to the original). Often fractals are found in nature, for example, when we see the outline of a cloud, the forms produced by lightning, snowflakes, the shape of a cauliflower and especially the morphology of surfaces appear as fractal objects (Figure 21).

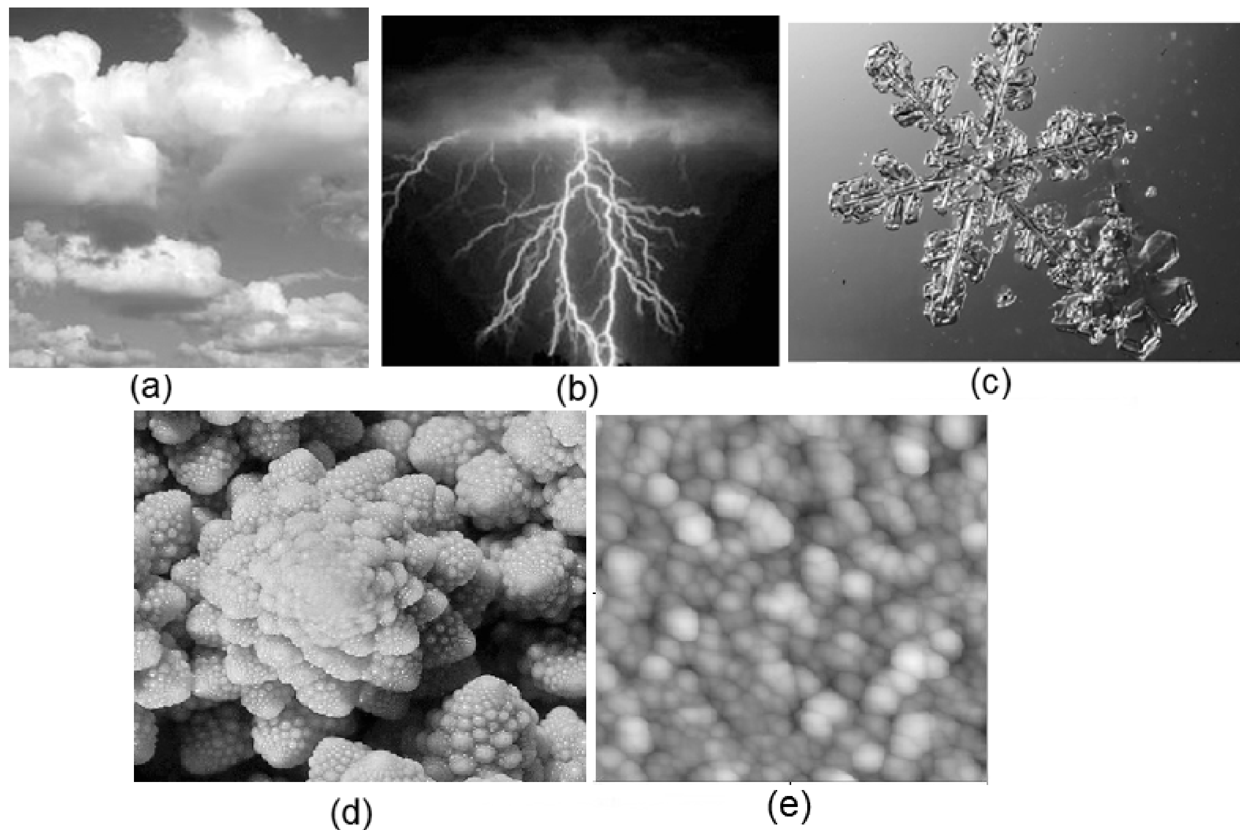

Fig. 21. Fractals in nature. (a) Outline of a cloud, (b) lightning, (c) snowflake, (d) surface of a cauliflower, (e) surface of a thin film of nickel oxide obtained AFM (Popsci, 2011; Saint-Marty Marty, 2011; Chaos Theory Dance, 2011).

9.1.1 Self-similar fractals

Self-similar fractals are figures that are completely invariant under scale transformations. An example of self-similar fractal is the Sierpinski Triangle (Figure 22) that does not change its shape under a scale transformation (Assis et al., 2008).

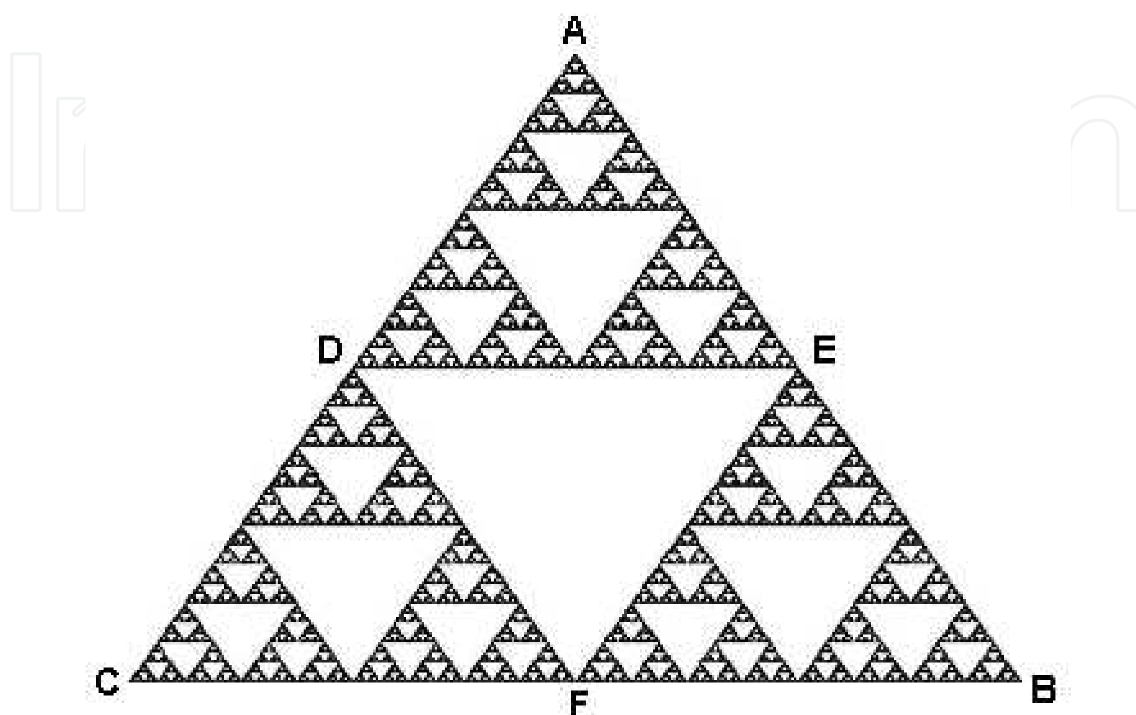

Fig. 22. The Sierpinski Triangle. The Triangle ADE is an exact copy in miniature of triangle ABC, depicting a self-similar fractal object. Triangles CDF and BEF are similarly related to triangle ABC (Assis et al, 2008).

9.1.2 Self-affine fractals

Self-affine fractals are a generalization of self-similar fractals. Self-affine fractal objects are composed of mini-copies of the original figure, but as the scale varies, the proportions are not maintained. Fractals are self-affine fractal invariant under anisotropic transformations. The surfaces of ultrathin films are often treated as self-affine fractal, since during the growth of the films there are two preferred directions of growth (Vicsek, 1989). Likewise most of the surfaces are classified as self-affine fractals.

9.1.3 The concept of dimension

The Euclidean dimension (D), popularly used, is a parameter that defines the geometry of an object. The Euclidean dimension is a parameter in the set of natural numbers in the interval [0, 3]. An object with D = 1, is associated with only one dimension, for example, a line. The dimension D = 2 describes plans objects and dimension D = 3 defines three-dimensional objects. Intuitively, D = 0 describes zero-dimensional objects, as a point, for example.

Not all objects are treated in the field of Euclidean geometry. For many of them can be given a semi-full scale, and this fact characterizes a fractal.

9.1.4 Fractal dimension to self-affine surfaces

Figure 23 represents a two-dimensional self-affine function. This function is defined in the interval [0, 1] and may represent, for example, the profile of a mountain.

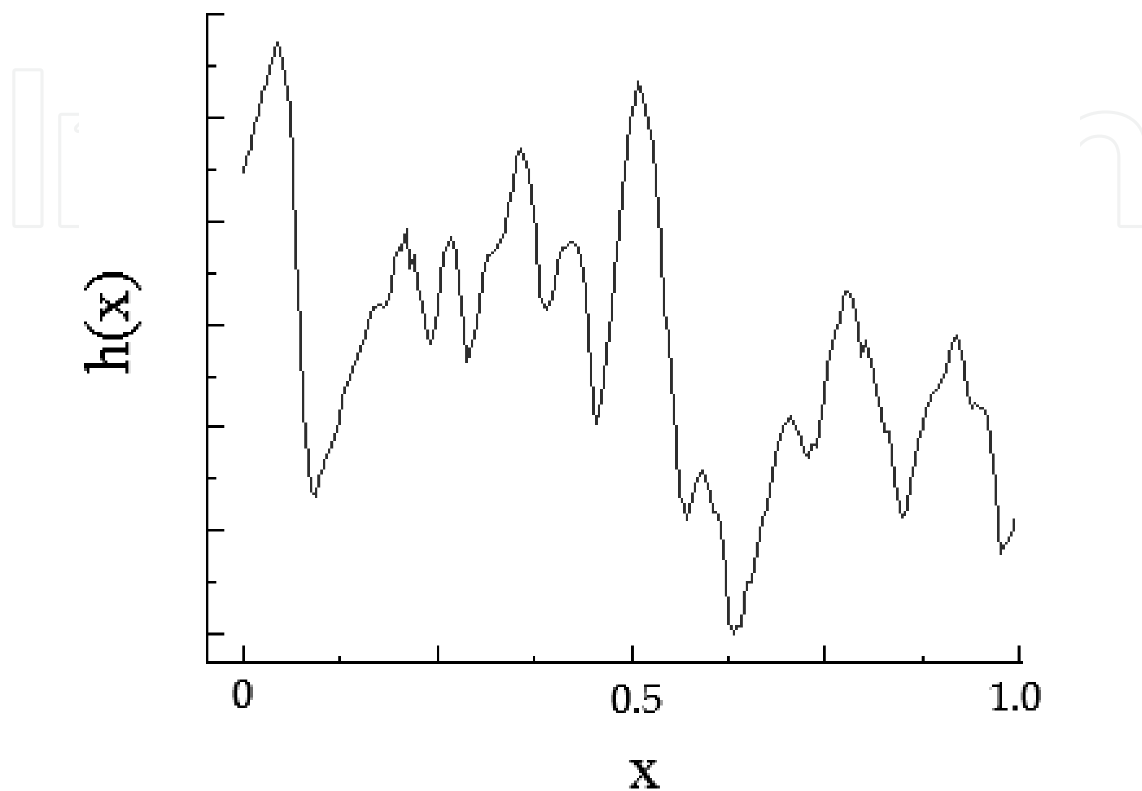

Fig. 23. Hypothetical self-affine function, h (x) represents the height h at position x, with x defined on the interval [0, 1]

Considering the object of study in this chapter, the surface has two preferred directions, one perpendicular to the surface where the roughness characterized by the height parameters, and the other along it. Since the scale is different between the two preferred directions, characterizing the object is an anisotropic transformation (Jurecka et al., 2010). To illustrate the anisotropic transformation, let's imagine that a self-affine surface, described by the function h(x) and expanded by a factor b in the surface dimension ($x \rightarrow bx$) then the dimension in the direction of growth must then be magnified by a factor b^{α} (leading $h \rightarrow b^{\alpha}h$). This way one can identify the similarities between the original surface and enlarged. Thus preserving the characteristics of an invariant transformation we have (Barabási & Stanley, 1995):

$$h(x) \sim b^{-\alpha} h(bx) \tag{14}$$

Where α, the roughness exponent, provides a quantitative measure of the imperfections of the surface morphology.

Equation (14) provides us with the information that an auto-order of this type is resized horizontally by a factor b, the vertical is just a different factor of b^{α}. In self-affine fractal objects, the difference between the two points vertically obeys the relation (14), generating (Barabási & Stanley, 1995):

$$\Delta h(x) \sim \Delta x^{\alpha} \tag{15}$$

Besides the roughness exponent, we can determine other fractal characteristics such as the fractal dimension of self-related functions through methods such as the Box Counting method (Barabási & Stanley, 1995).The profile function h(x) shown in Figure 23 can be embedded within a dimension D = 2. To obtain the fractal dimension through Box Counting method, we can fill this space with objects of equal size to the Euclidian space. Thus, our measuring elements are elements of area with side Δx and area Δx^2. To find the amount of information necessary to cover the function, divide the domain of the function in N_s segments, each of length $\Delta x = 1/N_s$. Making use of equation (15) will require $\Delta h/\Delta x \sim \Delta x^{\alpha-1}$ to cover the function. Finally, the total number of measurement objects to cover the entire function will be:

$$N(\Delta x) \sim N_s.\Delta x^{\alpha-1} \tag{16}$$

Considering $\Delta x = 1/N_s$ thus:

$$N(\Delta x) \sim \Delta x^{\alpha-2} \tag{17}$$

From the definition of Fractal Dimension we have (Cruz et al., 2002):

$$D_f = \lim_{\Delta x \to 0}\left(\frac{\ln N(\Delta x)}{\ln(1/\Delta x)}\right) \tag{18}$$

The equation (18) for an object of dimension D becomes:

$$D_f = D - \alpha \tag{19}$$

Equation (19) shows that the surface roughness is closely linked with the fractal dimension. Thus, by knowing the surface roughness exponent one can obtain the fractal dimension.

9.1.5 Fractal dimensions using SPMs techniques

The techniques of scanning probe microscope allow us to find the roughness of surfaces. Figure 24 represents particles striking a one-dimensional surface. Each square represents one particle. The size of the surface in the horizontal direction is defined by an L number of squares.

Using a mathematical tool and the Root Mean Square (RMS roughness) we can find the surface roughness (R_q) using the concepts of Laws Scale (Cruz et al., 2002; Lagally, 1990). In this case, the roughness follows the discrete growth model, shown in Figure 24 as a function of the time and the RMS function is rewritten as (Barabási & Stanley, 1995):

$$R_q^2(L,t) \equiv \frac{1}{L}\sum_{x=1}^{L}\langle\left[h(x,t) - \langle h_L(x,t)\rangle\right]^2\rangle_x \tag{20}$$

Where h(x, t) is the height of the column at x at time t. The term $\langle h_L(x, t)\rangle$ is the average height of a given observation window L, whereas the brackets $\langle\ldots\rangle_x$ encompass the spatial

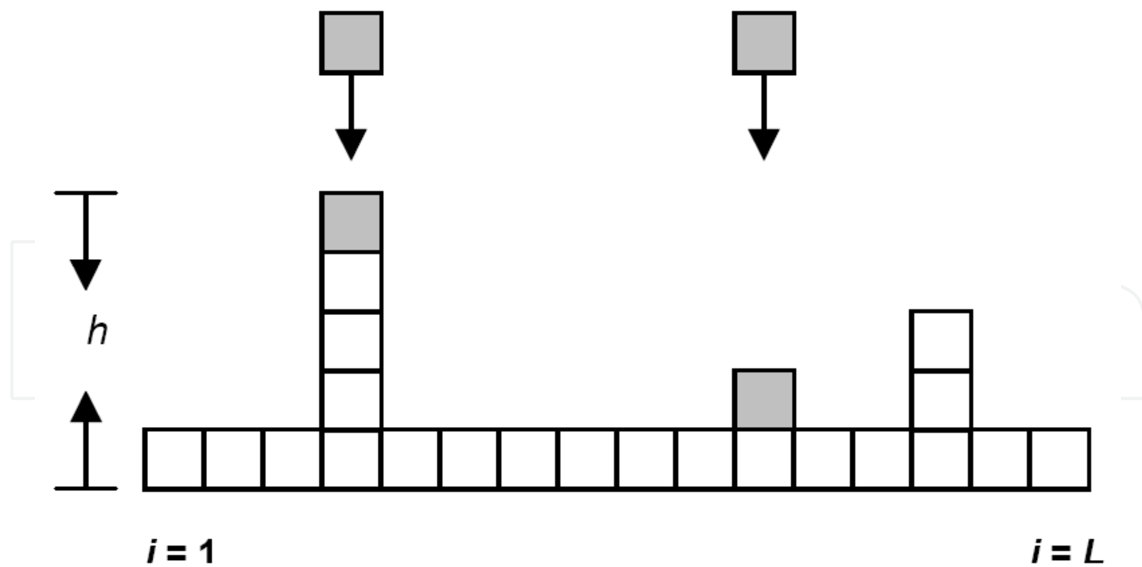

Fig. 24. Diagram illustrating the formation of a surface. Each square represents a particle arriving at this surface (Cruz T.G.S., 2002).

average in x, for all windows of the same size, and averaged over all windows chosen. Using the concepts of fractals, the self-affine function h(x) in this case can be compared to roughness function R(L). Thus, analogously to equation (15) we have:

$$R(L) \sim L^{\alpha} \tag{21}$$

Using equation 20 and plotting a graph of the logarithm of the values obtained from microscopic observations as a function of L we can obtain the roughness exponent α.

Figure 25 is an example of a graph of R_q versus L. For self-affine surfaces, the slope of the roughness in the region of non-saturated is the roughness exponent.

Thus, the roughness exponent can be found and provide the fractal dimension by equation (17).

9.2 Power spectral density (PSD)

The power spectral density (PSD) is a complementary analysis of surface roughness which gives information related to parameters of the roughness height and spacing. The PSD is a parameter used in micrographs which relates the Fourier Transform (FT) with the root mean square roughness (RMS). The relationship between the PSD, FT and RMS is described by (Park, 2011):

$$PSD = FT^2 = RMS^2 \tag{22}$$

A Discrete Fourier Transform (DFT) used for a 3D topography can be described by (Czifra & Horvath, 2011):

$$F(p_k, q_l) = \Delta y . \Delta x \sum_{d=1}^{N} \sum_{c=1}^{M} z(x_c, y_d) e^{-i2\pi(x_c p_k + y_d q_l)} \tag{23}$$

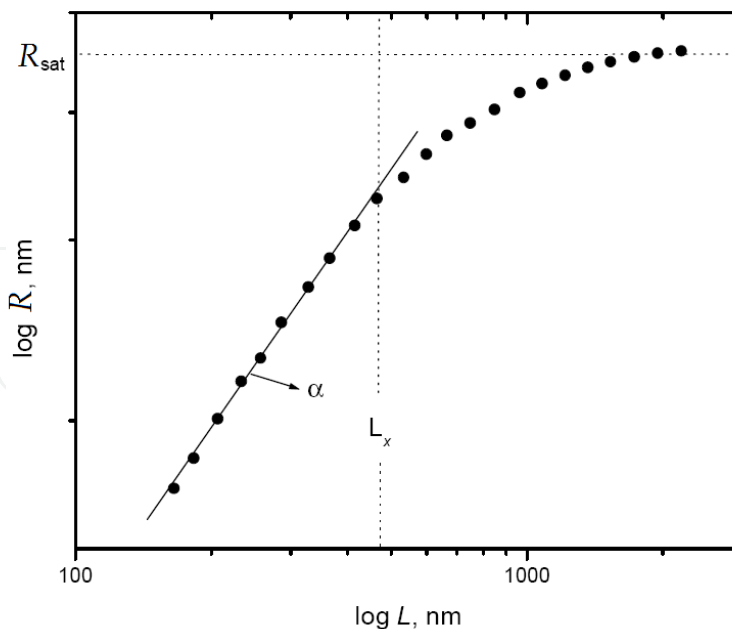

Fig. 25. For self-affine surfaces, the slope of the unsaturated region of roughness is the roughness exponent (Cruz T.G.S., 2002).

Where p_k is the kth frequency in direction x; q_l is the lth frequency in direction y, z(x_c, y_d) is the height coordinate located at x_c, y_d, M is the number of points in the profile, N is the number of profiles, Δx, Δy, are sampling distances, i is the imaginary unit (Czifra & Horvath, 2011).

The PSD is able to separate the surface profile at various wavelengths, that is, the sum of the wavelengths generated by the PSD, make up the original form of the surface profile by a Fourier analysis (Figure 26). This information is relevant in discerning how each component contributes to the original surface.

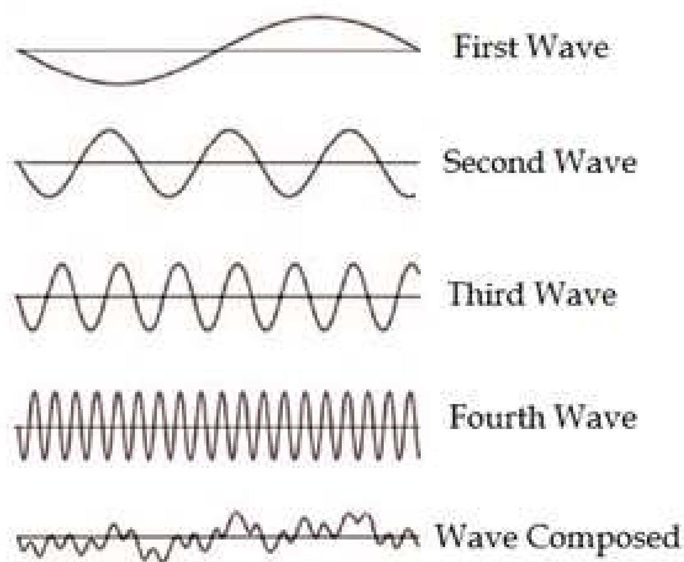

Fig. 26. Example of a wave decomposed by PSD. The sum of the four waves results in the composed wave (adapted from Freitas, A. C. P., 2010).

In the example given in Figure 26, the composed wave equation is the sum of each of the four waves. The surface can thus be divided into height parameters and parameters of wavelength. The figure shows that the first wave contributes to the larger waves while the fourth wave contributes to reduced ripples

10. References

Analytical Sciences Digital Library - Wilson, R. A., & Bullen, H. A. (2007). Introduction to Scanning Probe Microscopy. Department of Chemistry, Northern Kentucky University, Highland Heights, KY 41099. Accessed 10;03;2011. Available from <*http://asdlib.org/*>.

Assis, T. A., Miranda, J. G. V., Mota, F. B., Andrade, R. F. S., & Castilho, C. M. C. (2008). Geometria fractal: propriedades e características de fractais ideais. *Revista Brasileira de Ensino de Física*, Vol. 30, No 2. (jul 2008) pp. 2304-2314, 1806-1117.

B.C. MacDonald & Co. Accessed 10; 03; 2011. Available from <*http://www.bcmac.com/*>.

Barabási, A. L., & Stanley, H. E. (1995). *Fractal Concepts in Surface Growth*, Cambridge University Press, 0-521-48318-2, Cambridge

Binnig, G., Quate, C. F., & Gerber, C. (1986). Atomic Force Microscope. *Physical Review Letters*, Vol. 56, No 9, (mar. 1986) pp. 930-933, 0031-9007.

Binning, G., Rohrer, H., Gerber, C., Weibel, E. Surface Studies by Scanning Tunneling Microscopy. *Physical Review Letters*, Vol 49, No 1, pp. 57-61, 0031-9007.

Bowen, W.R., Hilal, N., Lovitt, R.W., & Wright, C.J. (1998). A new technique for membrane characterization: Direct measurement of the force of adhesion of a single particle using an atomic force microscope. *Journal of Membrane Science,* Vol. 139, No 2, (feb. 1998), pp. 269-274, 0376-7388.

Chaos Theory Dance. Accessed 10;03;2011. Available from <*http://www.chaostheorydance.com/*>.

Cruz, T.G.S. (2002) Leis de Escala e Dimensão Fractal em Filmes Finos: Microscopia de Força Atômica e Técnicas Eletroquímicas. 131 p. Thesis (PhD in physics) – State University of Campinas, UNICAMP, Brazil, Campinas, sep 2002.

Cruz, T.G. S., Kleinke, M.U., & Gorenstein, A. (2002). Evidence of local and global scaling regimes in thin films deposited by sputtering: An atomic force microscopy and electrochemical study. *Applied Physics Letters*, Vol. 81, No 26, (dec. 2002), pp. 4922-4924, 0003-6951.

Czifra, A., & Horvath, S. (2011). Complex microtopography analysis in sliding friction of steel-ferodo material pair. *Meccanica.* Vol. 46, No. 3, (jun 2011), pp. 609-616, 1572-9648.

Freitas, A. C. P. (2010) Influencia do tipo de polimento pós-clareamento na alteração de rugosidade, cor e brilho da superfície de esmalte dental humano. 110 p. Thesis (Phd in Dentistry) – University of São Paulo, USP, Brazil, São Paulo, 2010

Gadelmawla, E.S., Koura, M.M., Maksoud, T.M.A., Elewa, I.M., Soliman, H.H. (2002). Roughness Parameters, *Journal of Materials Processing Technology*, Vol. 123, No 1, (apr. 2002), pp. 133-145, 0924-0135.

Guisbiers, G., Van Overschelde, O., Wautelet, M., Leclere, Ph., & Lazzaroni, R. (2007). Fractal dimension, growth mode and residual stress of metal thin films. *Journal of Physics D-Applied Physics*, Vol. 40, No 4, (feb. 2007), pp. 1077-1079, 0022-3727.

Heintze, S.D., Forjanic, M., & Rousson, V. (2006). Surface roughness and gloss of dental material as a function of force and polishing time in vitro. *Dent Mater*, Vol. 22, No 2, (feb. 2006), pp. 146-165, 1608-4582.

Howland, R. & Benatar, L., (2000). A Practical Guide to Scanning Probe Microscopy, in, *Penn State Polymer Physics Group*, Accessed 10;03;2011, Available from <*http://raman.plmsc.psu.edu/*>.

Jurecka, S., Kobayashi, H., Takahashi, M., Matsumoto, T., Jureckova, M., Chovanec, F., & Pincik, E. (2010). On the influence of the surface roughness onto the ultrathin SiO(2)/Si structure properties. *Applied Surface Science*, Vol. 256, No 18, (jul 2010), pp. 5623–5628, 0169-4332.

Lagally, M. G. (1990). *Kinetics of Ordering and Growth at Surfaces*, Plenum Press, 978-0306437021, New York.

Liu, D.-L., Martin, J., & Burnham, N.A. (2007). Optimal roughness for minimal adhesion. *Applied Physics Letters*, Vol. 91, No. 4, (Jul. 2007), pp. 31071-31073, 0003-6951.

MikroMasch. Accessed 10; 03; 2011. Available from <*http://www.spmtips.com/*>.

Mandelbrot, B. B. (1982). *Fractal Geometry of Nature*, Freeman, 978-0716711865, San Fracisco.

Nagel, H. D. (1988). Limitations in the determination of total filtration of X-ray tube assemblies. *Physics in Medicine and Biology*, Vol. 33, No 2, (feb. 1988), pp. 271-289, 0031-9155.

Oberg, E., Jones, F. D., Horton, H. L., & Ryffel, H. H. (2000). *Machinery`s handbook* (26th ed.), Industrial Press Inc., 978-1-59124-118-8, New York.

Odom, T. W., (2004). Laboratory manual, Nanoscale pattern and systems, in, *The Odom Group*, Accessed 10;03;2011, Available from <*http://chemgroups.northwestern.edu/odom/*>.

Park Systems. Accessed 10; 03; 2011. Available from <*http://www.parkafm.co.kr/*>.

Popular Science. Accessed 10; 03; 2011. Available from <*http://www.popsci.com*>.

Precision Devices, Inc. Accessed 10;03;2011. Available from <*http://www.predev.com/*>.

Raoufi, D. (2010). Fractal analyses of ITO thin films: A study based on power spectral density, *Physica B*, Vol. 405, No 1, (jan 2010), pp. 451–455, 0921-4526.

Rugar, D.,Hansma, P. (1990). Atomic Force Microscopy, *Physics Today*, Vol. 43, No 10, (oct. 1990), pp. 23-30, 0031-9228.

Sainty Marty-Marty. Accessed 10;03;2011. Available from <*http://saintmarty-marty.blogspot.com/*>.

Schitter, G., Astrom, K.J., DeMartini, B.E., Thurner, P.J., Turner, K.L., Hansma, P.K. (2007). Design and Modeling of a high-speed AFM-scanner . *IEEE Transacions on Control Systems Technology*, Vol. 15, No 5, (sep. 2007), pp. 906-915, 1063-6536.

Stears, J. G., Felmlee, J. P., & Gray, J. E. (1986). Half-Value-Layer increase owing to tungstein buildup in the X-ray tube: fact or fiction. *Radiology*, Vol. 160, No 3, (sep. 1986), pp. 837-838, 3737925.

Vicsek, T. (1989). *Fractal Growth Phenomena* (2nd ed), World Scientific, 981-0206690, New Jersey.

Vorburguer, T. V., & Raja, J., (1990). Surface Finish Metrology Tutorial, in, *Nist Calibrations*, NISTIR 89-4088

Takikawa, R., Fujita, K., Ishizaki, T., & Hayman, R.E. (2006). Restoration of post-bleach enamel gloss using a non-abrasive, nano-hydroxyapatite conditioner, *Proceedings*

of 84th General Session & Exhibition of the IADR, ISBN, Brisbane-Australia, June 28-July 1.

Thomas, T.R. (1999). *Rough Surfaces* (2nd ed), Imperial College Press, 978-1-86094-100-9, London.

Torkhov, N. A., & Novikov, V. A. (2009). Fractal geometry of the surface potential in electrochemically deposited platinum and palladium films. *Semiconductors*, Vol. 43, No 8, (aug 2009), pp. 1071–1077, 1063-7826.

Whitehouse, D.J. (1975) "Stylus Techniques", in Characterization of Solid Surfaces, P.E. Kane and G.R. Larrabee, eds. Plenum Press, New York , p. 49.

Wiesendanger, R. (1994). *Scanning Probe Microscopy and Spectroscopy*, Cambridge University Press, 0-521-42847-5, Cambridge.

Yadav, R.B S., Papadimitriou, E.E., Karakostas, V.G., Shanker, D., Rastogi, B.K., Chopra, S., Singh, A. P., & Kumar, S. (2011). The 2007 Talala, Saurashtra, western India earthquake sequence: Tectonic implications and seismicity triggering. *Journal of Asian Earth Sciences*, Vol. 40, No 1, (jan 2011), pp. 303-314, 1367-9120.

Yoriyaz, H., Moralles, M., Siqueira, P.T.D., Guimarães, C.C., Cintra, F.B., & Santos, A. (2009). Physical models, cross sections, and numerical approximations used in MCNP and GEANT4 Monte Carlo codes for photon and electron absorbed fraction calculation. *Medical Physics,* Vol. 36, No 11, (oct. 2009), pp. 5198-5213, 0094-2405.

Zygo Corporation. Accessed 10;03;2011. Available from <*http://www.zygo.com/*>.

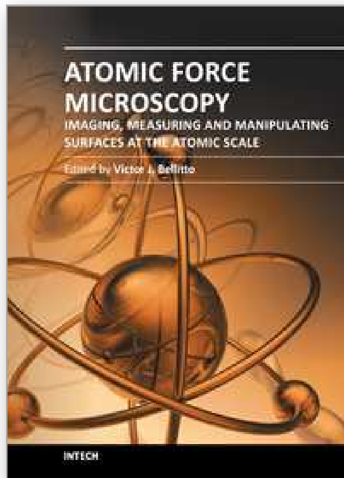

Atomic Force Microscopy - Imaging, Measuring and Manipulating Surfaces at the Atomic Scale
Edited by Dr. Victor Bellitto

ISBN 978-953-51-0414-8
Hard cover, 256 pages
Publisher InTech
Published online 23, March, 2012
Published in print edition March, 2012

With the advent of the atomic force microscope (AFM) came an extremely valuable analytical resource and technique useful for the qualitative and quantitative surface analysis with sub-nanometer resolution. In addition, samples studied with an AFM do not require any special pretreatments that may alter or damage the sample and permits a three dimensional investigation of the surface. This book presents a collection of current research from scientists throughout the world that employ atomic force microscopy in their investigations. The technique has become widely accepted and used in obtaining valuable data in a wide variety of fields. It is impressive to see how, in a short time period since its development in 1986, it has proliferated and found many uses throughout manufacturing, research and development.

How to reference
In order to correctly reference this scholarly work, feel free to copy and paste the following:

R.R.L. De Oliveira, D.A.C. Albuquerque, T.G.S. Cruz, F.M. Yamaji and F.L. Leite (2012). Measurement of the Nanoscale Roughness by Atomic Force Microscopy: Basic Principles and Applications, Atomic Force Microscopy - Imaging, Measuring and Manipulating Surfaces at the Atomic Scale, Dr. Victor Bellitto (Ed.), ISBN: 978-953-51-0414-8, InTech, Available from: http://www.intechopen.com/books/atomic-force-microscopy-imaging-measuring-and-manipulating-surfaces-at-the-atomic-scale/measurement-of-the-nanoscale-roughness-by-atomic-force-microscopy-basic-principles-and-applications

INTECH
open science | open minds

InTech Europe
University Campus STeP Ri
Slavka Krautzeka 83/A
51000 Rijeka, Croatia
Phone: +385 (51) 770 447
Fax: +385 (51) 686 166
www.intechopen.com

InTech China
Unit 405, Office Block, Hotel Equatorial Shanghai
No.65, Yan An Road (West), Shanghai, 200040, China
中国上海市延安西路65号上海国际贵都大饭店办公楼405单元
Phone: +86-21-62489820
Fax: +86-21-62489821

© 2012 The Author(s). Licensee IntechOpen. This is an open access article distributed under the terms of the Creative Commons Attribution 3.0 License, which permits unrestricted use, distribution, and reproduction in any medium, provided the original work is properly cited.

IntechOpen

IntechOpen